Confidence-based Design Optimisation of Belt Limiting Force Using Gaussian Process Model Prediction of Rib Fracture Risk.

Changmin Baek, Jungsu Kim, Junik Cho, Jingwen Hu, Dongjin Lee

Abstract This study presents a confidence-based design optimisation (CBDO) framework that accounts for both metamodel and input uncertainties to minimise head excursion while satisfying thoracic injury constraints. First, the GHBMC 50th percentile male model was validated against three distinct post-mortem human subject configurations. Using this validated baseline crash condition, parametric crash simulations were conducted—varying torso angle, D-ring height, belt limiting force, and H-point position—to generate injury prediction data across diverse occupant postures and restraint configurations. A Gaussian process metamodel model was then trained by the resulting data and integrated into the CBDO framework to find an optimal design that accounts for both input uncertainty and metamodel uncertainty. This framework successfully identified an uncertainty-informed optimum using 48 computational simulations, demonstrating its practical efficiency for reliable restraint system design.

Keywords Gaussian process surrogate, Human body models, Confidence-based design optimisation, Uncertainty inputs, Uncertainty quantification.

I. INTRODUCTION

Human body models (HBMs) offer greater biofidelity than traditional anthropomorphic test devices (ATDs), such as Hybrid III, by accurately replicating human anatomy, diverse passenger postures and body types [1-2]. The European New Car Assessment Programme (Euro NCAP) plans to include HBM-based virtual crash simulations in addition to conventional ATD crash tests [3]. Standard regulatory and consumer information tests evaluate only a limited set of predefined scenarios [3]. Consequently, restraint systems that perform well in these tests may not fully capture performance across the broader range of real-world conditions, particularly those involving personalised seating configurations (e.g., varying postures, seat positions, and belt anchors) [4-5]. Evaluating this wide range of configurations with HBMs typically requires Monte Carlo simulations (MCS) [6], but a single HBM simulation can take several hours, making the large number of iterations typically needed for MCS computationally prohibitive. Metamodels [7–11], which here refer to data-driven predictive models, can address these computational bottlenecks by approximating injury responses from a limited number of HBM simulations. Among the available meta models, Gaussian process (GP) models have demonstrated high predictive accuracy for the highly nonlinear kinematics and injury metrics in biomechanical applications [12-13].

Metamodels inherently involve uncertainty prediction because they are trained on a finite number of samples and may not fully capture the true response surface across the entire input space. Additional sources of uncertainty may arise from simulation noise, numerical discretisation, modelling assumptions, and variability in the training data. Conventional deterministic design optimisation (DDO) seeks to improve nominal performance without accounting for these uncertainties, whereas reliability-based design optimisation (RBDO) accounts for input variable uncertainty but assumes the metamodel as an exact representation of the true response. Confidence-based design optimisation (CBDO) extends RBDO by accounting for both input uncertainty and metamodel uncertainty, thereby identifying designs that remain reliable even when predictions are imprecise [14-15]. To the authors' knowledge, CBDO has not yet been applied in the biomechanics domain, where injury prediction exhibits substantial variability and is often associated with high computational cost, especially with HBM simulations, which can severely limit the training data available for metamodel development.

D. Lee (e-mail: dlee46@hanyang.ac.kr) is an Assistant Professor, C. Baek is a PhD student, and J. Kim and J. Cho are MS students, all in the Department of Automotive Engineering at Hanyang University, Seoul, South Korea. J. Hu (e-mail: jwhu@umich.edu) is a Research Professor at the University of Michigan Transportation Research Institute (UMTRI), MI, USA.

In frontal impact restraint optimisation, a primary trade-off exists between thoracic protection and head protection, as lowering belt force limits can reduce chest loading at the expense of increased head excursion [16–18]. This main trade-off between controlling head movement and reducing chest loading happens differently in different seats. Front seats must balance chest loads against the airbag bottoming out, while rear seats focus on stopping the head from hitting the front seat. However, the basic optimization challenge is the same for all frontal impact designs, meaning our simplified baseline setup is useful for both environments. As variability in occupant posture (e.g., torso angle and H-point position) can influence this injury balance [19], deterministic optimisation for a single nominal configuration may not be sufficient. Accordingly, a framework that propagates both occupant-related uncertainty and metamodel prediction uncertainty is needed to ensure that the selected restraint design remains protective across a realistic range of seated postures.

This study presents a CBDO framework using a GP model to optimise D-ring height and shoulder-belt force limit. The primary objective is to minimise head excursion while satisfying probabilistic thoracic injury constraints under occupant variability. A 50th-percentile male GHBMC model was first validated against post-mortem human subject (PMHS) frontal sled test data to ensure kinematic and rib-level accuracy. Using this validated baseline, we conducted parametric simulations across a range of postures and restraint configurations to generate an injury response dataset. Subsequently, a GP trained on this data was integrated into the CBDO framework to identify an optimal restraint design that remains robust under occupant variability. The main contributions of this study are; (1) bridging the gap between computationally intensive HBM simulations and uncertainty-aware restraint design via CBDO; (2) quantifying the combined effects of occupant variability and metamodel uncertainty; and (3) highlighting potentially non-intuitive relationships between belt force and thoracic injury.

II. METHODS

Baseline Finite Element Modelling for PMHS Test

We constructed a GHBMC M50-OS v2-3-based frontal sled test model to reproduce the experimental results [20-21] from frontal impact tests conducted at the University of Virginia using three male PMHS (weight = 68 ± 2 kg, height = 1,780 ± 50 mm). A frontal sled model was obtained from OpenVT and used as the simulation environment. The sled model consisted of a rigid seat plate, footrest, knee bolster, and a 3-point seatbelt system

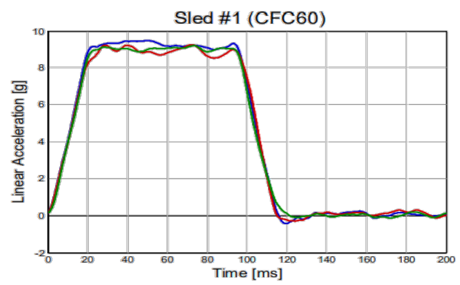

(a) 9g sled impact pulse.

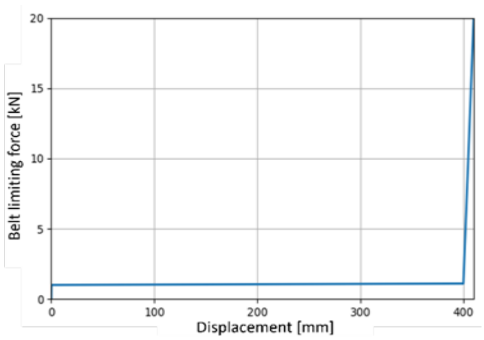

(b) 1D load limiter belt curve.

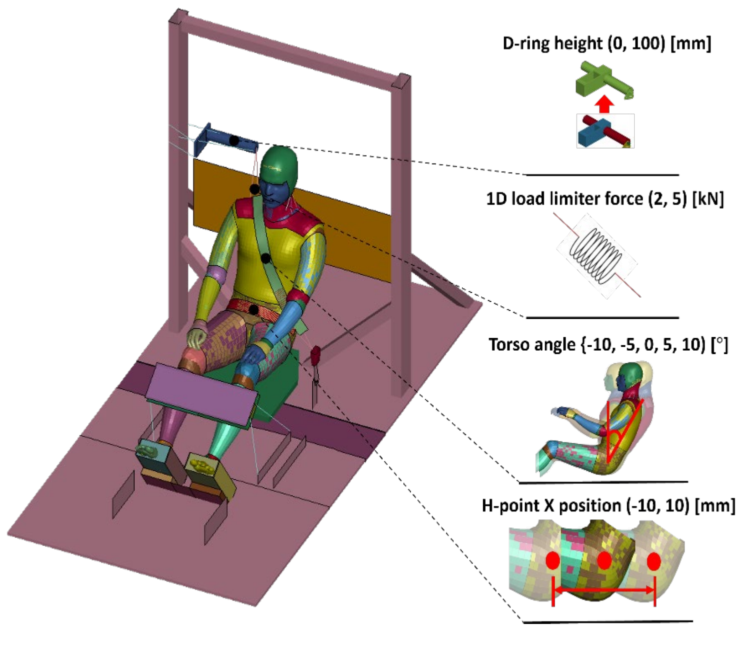

(c) Sled model configuration (*left*) and four input variables (*right*)

Fig. 1. Baseline frontal sled model and input conditions used for parametric simulations. The figure shows: (a) the sled pulse acceleration applied in the baseline simulation; (b) force-displacement characteristics of the 1D discrete load limiter used to define the belt limiting force profile during payout; and (c) the sled model configuration and the four input variables used for the DOE: torso angle, D-ring height, load limiter force, and H-point position.

equipped with a 3 kN load limiter. This sled configuration was selected because it provides a highly controlled chest-loading environment for examining belt-force effects. A 9 g frontal impact pulse was applied as the boundary condition. The occupant posture was prescribed by setting the upper-body and lower-body postures to specific target angles. The initial upper-body posture was defined by a torso angle of 24°, measured relative to the frontal plane along a line connecting the centers of attachment of the second and fourth ribs on the sternum. For the lower body, the femur and tibia were positioned such that their angles relative to the horizontal line were 11.4° and 33.8°, respectively. The H-point was positioned with the greater trochanter 101.6 mm from the rear seat edge in the x-direction and 101.6 mm above the seat plate in the z-direction. The hands were positioned on the thighs. Figure 1 shows the constructed sled model configuration, with the sled impact pulse curves and the force displacement curve of the 1D discrete load limiter. We validated the constructed model using the Ellipse and DALW scores proposed by Euro NCAP for HBM assessment [22-23]. The baseline validation served to confirm the reliability of the newly assembled sled-HBM environment, providing a trusted benchmark before generating the parametric simulation set for the injury variability investigation.

Design of Experiments

Using the validated baseline model, we generated a parametric simulation dataset by systematically varying four input variables: torso angle X_1, D-ring height X_2, belt limiting force X_3, and H-point X position X_4. D-ring height and belt-limiting force were selected as the primary design variables for system optimisation, while torso angle and H-point position were designated as uncertain variables to evaluate framework robustness. These parameters are the most critical for upper-body kinematics; secondary variables were excluded. The parameter bounds reflect realistic design and positioning limits established from literature and engineering judgment. Posture variations align with real-world seating [24]; load limiter bounds (2–5 kN) span modern progressive adaptive systems [25-26].

A 50 km/h crash pulse was applied by scaling the original 30 km/h impact pulse to extend the analysis beyond the loading conditions used in the Gold Standard test series [27], which served as the validation reference. This scaling was performed because the original baseline impact pulse did not induce sufficiently severe injury responses to bound and evaluate the optimization problem. Torso angle was treated as a discrete variable with five levels ranging from -10° to 10°, while the remaining three variables were defined as continuous variables: D-ring height (0-100 mm), belt limiting force (2-5 kN) and H-point X position (-10-10 mm). The load limiter was modelled as a 1D discrete element; its restraining force was the design variable, with deformation range fixed. These model configurations are shown in Fig. 1. Fig. 2 illustrates how the torso angle and H-point position were implemented in the HBM. These ranges span a wide spectrum of real-world seating postures (forward- or rearward-leaning) under a single frontal impact condition.

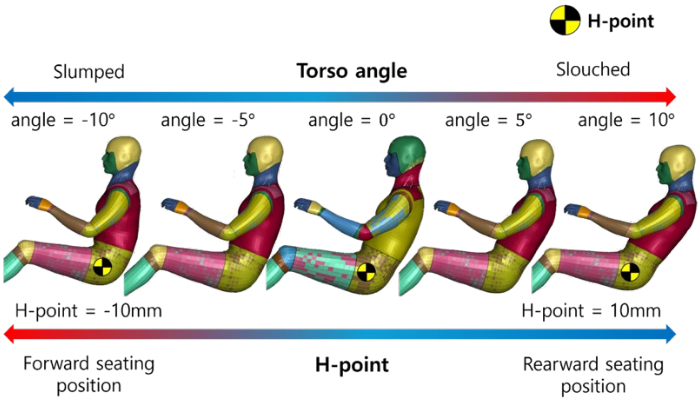

Fig. 2. Diverse occupant seating postures were generated by varying the torso angle and H-point position in the GHBMC model. Positive torso angle values corresponded to a more slouched posture, whereas negative values represented a more slumped posture. For H-point position, larger positive values indicated a more rearward seating position, while larger negative values indicated a more forward seating position.

The posture adjustment was performed via a pre-simulation positioning procedure in Oasys PRIMER. When the torso angle was varied, head and neck positions were adjusted to keep the head CoG X/Z coordinates relative to C6 consistent with the baseline. Both positioning variables were defined relative to their respective validated baseline coordinates. Following the adjustment of the H-point position, the knee bolster was rigidly attached to the occupant model during the setting simulation to preserve anatomical alignment. From each simulation, we extracted two response variables: maximum X direction head excursion ($u_{hX,\max}$) and the risk of sustaining three or more rib fractures for a 50-year-old occupant, denoted as NFR3+(50) [28].

Training a metamodel on limited data requires a robust space-filling sampling strategy. A common guideline for GP construction suggests a minimum of 10 samples per input dimension [29], yielding a baseline of 40 points for the four-variable input space considered here. We therefore generated a total of 40 samples, representing a practical balance between the sampling needs of GP modelling and the substantial computational cost associated with each HBM simulation (approximately seven hours per run on an Intel Xeon Gold 6526Y processor, using LS-DYNA MPP single-precision R12.0.0 with 16 cores). All input variables were sampled independently to construct a space-filling design domain for efficient GP training. Since torso angle is discrete, purely random sampling could lead to an uneven distribution across its five levels. To ensure balanced sampling, sample vectors $\mathbf{z}_i \in \mathbb{R}^3 (i = 1, \dots, 8)$, comprising the three continuous variables, were assigned equally to each torso-angle category. Within each category, conventional Latin hypercube sampling (LHS) [30-31] was deemed sub-optimal due to potential clustering. Instead, a maximin LHS [32], which maximises the minimum pairwise distance $\delta^{(m)}$, where $\delta^{(m)} = \min_{i \neq j} \left\| \mathbf{z}_i^{(m)} - \mathbf{z}_j^{(m)} \right\| \ (m = 1, \dots, 3000)$ was used. Designs were retained only if $\delta^{(m)} > \delta^*$, where δ^* represents the maximum distance found among all previous candidates (initialised at zero). Finally, the samples of the continuous variables associated with the derived δ^* were denormalised to their physical bounds, resulting in input vectors $\boldsymbol{x}$. The D-ring height and H-point X position were quantized in 1 mm increments, while belt limiting force was quantized in 100 N increments. This sampling strategy resulted in a final training dataset of $L = 40$ input-output pairs

$$\{\boldsymbol{x}^{(l)}, f_{hX,max}(\boldsymbol{x}^{(l)})\}_{l=1}^{L} \text{ and } \{\boldsymbol{x}^{(l)}, f_{NFR3+}(\boldsymbol{x}^{(l)})\}_{l=1}^{L} \tag{1}$$

where, the input data $\boldsymbol{x}^{(l)} = \left(x_1^{(l)}, x_2^{(l)}, x_3^{(l)}, x_4^{(l)}\right)$ represents the lth realisation of the uncertain input variables $X_i (i = 1, \dots, 4)$. The terms $f_{hX,max}(\cdot)$ and $f_{\text{NFR3+}}(\cdot)$ denote the simulation functions used to yield the corresponding output variables $u_{hX,max}$ and NFR3+(50), respectively. Fig. 3 presents the overall sampling process.

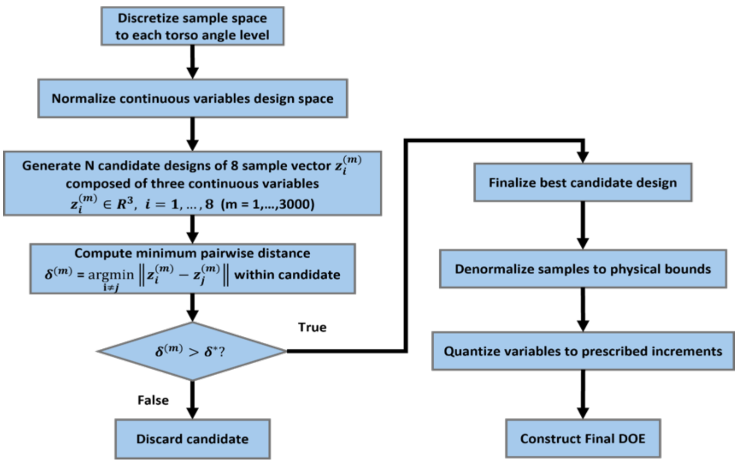

Fig. 3. Flowchart of the maximin LHS-based DOE sampling strategy.

Two Gaussian process (GP) metamodels with a Matérn kernel were trained on the L = 40 input–output pairs to predict head excursion and NFR3+(50). Kernel hyperparameters were tuned by leave-one-out cross-validation (LOOCV). Each prediction provides a posterior mean and variance used as the point estimate and uncertainty measure, respectively. The complete GP formulation is provided in Appendix E.

Confidence-based Design Optimisation

In this study, we used confidence-based design optimisation (CBDO). Torso angle (X_1) and H-point position (X_4) were treated as uncertain variables to account for variability in occupant posture, whereas D-ring height (X_2) and belt limiting force (X_3) were defined as design variables. To establish a baseline design, a deterministic design optimisation (DDO) problem was formulated as:

$$\begin{gathered}\min_{d} f_{hX,\max}(\mathbf{d}) \\ \text{subject to } f_{\text{NFR3+}}(\mathbf{d}) \leq 0.1, \\ 0 \leq d_1 \leq 100\text{ [mm]}; 2 \leq d_2 \leq 5\text{[kN]},\end{gathered} \tag{2}$$

where $f_{hX,\max}(\mathbf{d})$ represents the maximum head X excursion, and the $f_{\text{NFR3+}}(\mathbf{d})$ metric represents the probability that an average-sized occupant will not suffer a serious injury (AIS3 or higher) to the thoracic region. The performance constraint requires that the NFR3+(50) metric remains below 10% (0.1). The remaining constraints define the allowable deterministic design space for the D-ring height and belt limiting force. This DDO problem is solved iteratively, but the final optimised design is susceptible to significant reliability loss because it does not account for variability in the torso angle, H-point position, or manufacturing variations in the design variables.

To ensure robust design performance that explicitly accounts for both environmental uncertainty and model uncertainty, this study implements CBDO formulated as

$$\begin{gathered}\min_{d} \mathbb{E}\left[f_{hX,\max}(\mathbf{X},\mathbf{d})\right] \\ \text{subject to } \mathbb{P}(\mathbb{P}(f_{\text{NFR3+}}(\mathbf{X},\mathbf{d})) \leq 0.1) \geq R_t) \geq CL_t, \\ 0 \leq d_1 \leq 100\text{[mm]}; 2 \leq d_2 \leq 5\text{[kN]},\end{gathered} \tag{3}$$

where, $\mathbb{E}[\cdot]$ is the mean operator and $\mathbb{P}[\cdot]$ is the probability operator. The inner probability $\mathbb{P}\left(f_{\text{NFR3+}}(\mathbf{X},\mathbf{d})\right)$ is a distribution sampled from GP posterior paths via Monte Carlo. The target confidence level CL_t specifies the required probability that the realised system reliability exceeds the target reliability, thereby explicitly quantifying and controlling the risk associated with both variable fluctuations and imperfect model predictions. For this analysis, the target confidence level CL_t was set to 0.7 (70% confidence target).

To account for input uncertainty at each design point, Monte Carlo sampling was performed. In this process, the D-ring height (X_2) and belt limiting force (X_3) were modeled as normally distributed variables, with standard deviations defined as 3% of their respective mean values [9]. The torso angle (X_1) and H-point position (X_4) were modeled using uniform distributions and generated via Latin Hypercube Sampling (LHS). For these parameters, the variation was constrained to a physical range of [-10, 10], resulting in a calculated standard deviation of 5.774. Table I summarises the definition and statistical properties of these input random variables.

TABLE I

DEFINITION AND STATISTICAL PROPERTIES OF THE RANDOM VARIABLES

Random variables	Lower bound	Upper bound	Mean	Standard deviation	Probability distribution
Torso angle (X_1) [°]	-10	8	0	5.774	Uniform
D-ring height (X_2) [mm]	0	100	d_1	$0.03d_1$	Normal
Belt limiting force (X_3) [kN]	2	5	d_2	$0.03d_2$	Normal
H-point X position (X_4) [mm]	-10	10	0	5.774	Uniform

We used 10,000 input samples for the objective function evaluation and 10,000 for the constraint evaluation, chosen to ensure convergence while maintaining tractability.

We evaluated the objective function as the mean of the GP predictive means for head X excursion over the input samples at each design point. For constraint evaluation, we incorporated metamodel uncertainty by sampling GP posterior paths using both the predictive mean vector and covariance matrix. Multiple realisations of the NFR3+ response were generated from the GP posterior to capture model uncertainty. To reduce the computational cost of handling the large covariance matrix, we used the expansion optimal linear estimation method for dimensionality reduction [32-33].

For each generated GP path, we computed the reliability $\boldsymbol{R}$ as the proportion of input samples satisfying $\text{NFR3} + (50) \leq 0.10$ within that realisation, given by:

$$\boldsymbol{R}^{(k)} = \frac{1}{N}\sum_{n=1}^{N} \mathbf{1}\left(\mathbf{g}^{(k)}\left(\boldsymbol{x}^{(n)}\right) \le 0.10\right) \ (N = 10000) \tag{4}$$

where $\mathbf{1}(\cdot)$ is an indicator function that produces one when the condition inside the parenthesis is true (i.e., $g^{(k)}\left(x^{(n)}\right) \le 0.10$) and zero when the condition is false.

Accordingly, we obtained one reliability value for each GP path, resulting in a total of 10,000 reliability values for a single design point. These values form a reliability distribution that reflects metamodel uncertainty. In this study, the median of this reliability distribution was defined as R_m, and the confidence level (CL) was defined as the proportion of metamodel realisations satisfying $R \ge R_t$. In other words, CL represents the probability that the reliability at a given design point exceeds the target reliability when metamodel uncertainty is considered.

We performed the optimisation using the Differential Evolution (DE) algorithm. DE carried out a global search within the prescribed ranges of the design variables (d_1, d_2), and the objective function and constraints were evaluated at each candidate design point. If either R_m or CL fell below its target value, a penalty was imposed according to the degree of deficiency. The penalty terms were defined as follows:

$$P_{R_m} = \begin{cases} (0.9 - R_m), & \text{if } R_m < 0.9 \\ 0, & \text{if } R_m \ge 0.9 \end{cases} \tag{5}$$

$$P_{CL} = \begin{cases} (0.7 - CL), & \text{if } CL < 0.7 \\ 0, & \text{if } CL \ge 0.7 \end{cases} \tag{6}$$

where P_{R_m} and P_{CL} denote the penalty terms associated with the reliability metric R_m and the confidence level CL, respectively.

These penalty terms guided the optimisation toward minimising the objective within the feasible region. For the obtained optimal design point, the objective function, R_m, CL, and the quantile information of the reliability distribution were recalculated using the same Monte Carlo input samples and GP paths to verify the optimisation results. Fig. 4 presents the overall algorithm of the proposed CBDO framework.

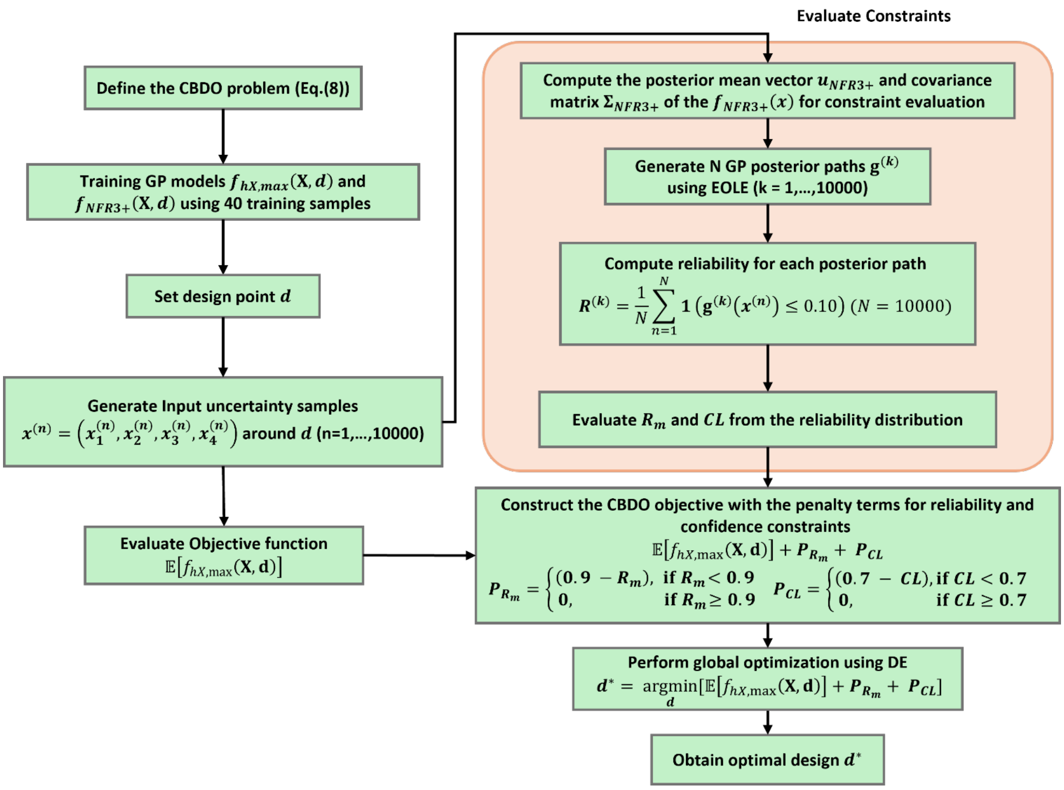

Fig. 4. Confidence-based design optimisation algorithm.

Finally, to evaluate the robustness of the DDO and CBDO optima, eight additional samples were generated around each initial optimum assigning different values to the uncertain variables and analysed, thereby expanding the training dataset to a total of 48 samples. The GP models were retrained on the expanded dataset and the optimal design points re-identified. In addition, for the optimal design point obtained at each stage, the objective function, reliability, and the influence of metamodel uncertainty were re-evaluated using 10,000 Monte Carlo input samples. Based on this procedure, we compared the performance of DDO and CBDO in terms of both the optimal objective value and the sensitivity of the optimum to additional data and its stability under uncertainty.

III. RESULTS

Baseline Model Validation

We validated the baseline model using the Ellipse and Dynamic Arc-Length Warping (DALW) scores used in the Euro NCAP framework. The Ellipse and DALW scores are validation metrics used to assess HBM simulation results against PMHS test responses. Although this framework was originally applied to a broad range of frontal, rear, and side sled tests for comprehensive HBM evaluation, in this study, the baseline model was validated using only the validation criteria corresponding to the Gold Standard 2 frontal sled condition. Validation was performed using the relative X, Y, and Z direction displacements of the head, T1, T8, and pelvis with respect to the sled, and the chest X-axis displacement. The baseline model satisfied all applicable validation criteria (Table AI in Appendix A).

Parametric relationships between input variables and output responses

Fig. 4 and Fig. B1 (Appendix B) present the relationships between the four input variables and the two output responses based on the initial 40 training samples. While torso angle, D-ring height, and H-point position lacked pronounced univariate effects (Fig. B1) – suggesting their roles are primarily governed by complex nonlinear interactions – belt limiting force appeared to have a dominant effect on both responses. Specifically, maximum head X-axis excursion exhibited an inverse relationship with belt limiting force (Fig. 4), decreasing across the design range. In contrast, NFR3+(50) displayed a non-monotonic trend: injury risk decreased as belt limiting force increased up to a certain threshold, beyond which risk increased again. This trend is counter-intuitive, as one would generally expect lower belt limiting forces to reduce the restraint load transmitted to the thorax and thereby mitigate thoracic injury risk; however, in this work, relatively high NFR3+(50) values were observed in some low belt limiting force cases.

To rule out the possibility that this counter-intuitive behaviour is an artifact of the retractor spool running out of webbing – which would cause an abrupt force spike unrelated to the intended load-limiting mechanism – the simulation set-up was carefully examined. The initial webbing length on the spool was set to 400 mm for all cases, and the shoulder-belt force–time histories were inspected across the entire design space. In this inspection, several low belt limiting force cases were found to exhibit a secondary force peak after the available webbing on the retractor spool was exhausted. This secondary force increase indicated spool bottoming-out, suggesting that the relatively high NFR3+(50) values observed in these low belt force cases were influenced by an abrupt restraint force that was not part of the intended load-limiting behaviour. Therefore, the relationship initially observed between belt limiting force and NFR3+(50) was considered to be partly influenced by the retractor payout limitation.

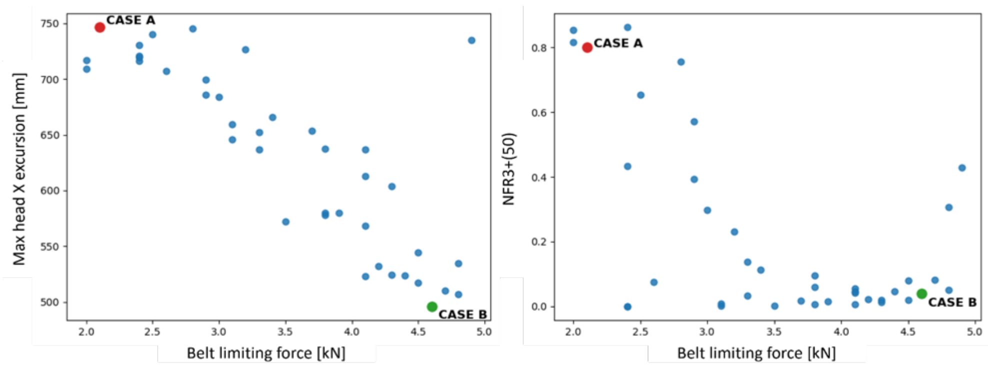

Fig. 4. Relationship between belt limiting force and the two response variables. CASE A and CASE B indicate the cases with the highest and lowest head excursion, respectively. The same two cases are highlighted in both plots to facilitate comparison of their corresponding injury response levels.

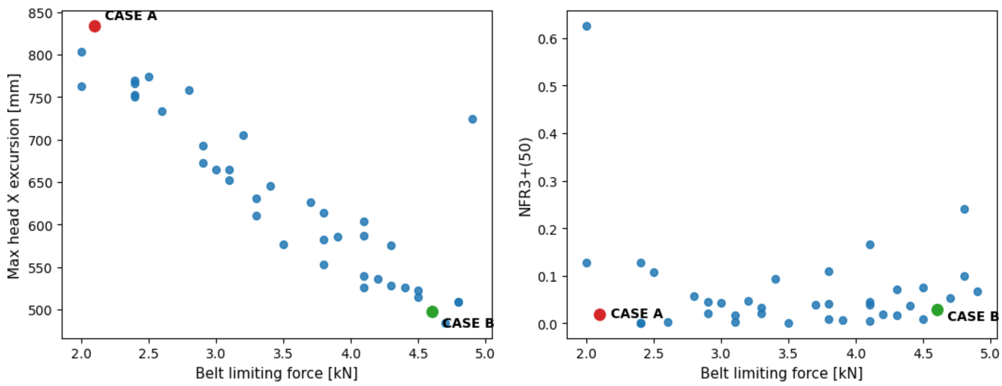

Fig. 5. Relationship between belt limiting force and the two response variables after eliminating bottoming-out. CASE A and CASE B correspond to the same cases in Fig 4.

Fig. F1 presents a comparison of occupant kinematics between CASE A (low belt limiting force in Fig. 4) and CASE B (high belt limiting force in Fig. 4) from side, top, and front views. In CASE A, the lower belt limiting force allows greater belt payout and less upper-body restraint, resulting in a translational motion pattern with pronounced forward flexion. In contrast, the higher belt force in CASE B produces a stronger torso restraint that limits forward translation while inducing a rotational motion about the belt anchorage.

To examine the effects of the variables under conditions in which bottoming-out did not occur, the allowable spool payout was increased to a level sufficient to prevent spool-out limitation. The converged spool payout observed in the case with the lowest belt limiting force was then applied consistently to all cases, and the simulations were repeated under this corrected payout condition. Fig. 5 and Fig. B2 (Appendix B) present the relationships between the four input variables and the two output responses based on the initial 40 training samples under non bottoming out condition.

In the corrected non-bottoming-out simulations, the high NFR3+(50) values previously observed in the low belt limiting force region were reduced. This indicates that the elevated thoracic injury risk in some low belt force cases was influenced by spool bottoming-out in the initial simulations. However, even after eliminating the bottoming-out effect, a clearly dominant inverse relationship between belt limiting force and NFR3+(50) was not observed across all low belt force cases.

Optimisation results with 40 training samples

Using the GP models trained on 40 samples, DDO and CBDO were performed. Predicted objectives were 595.3 mm (DDO) and 602.6 mm (CBDO), both satisfying the injury constraint. Because CBDO also enforces a confidence-based constraint, it searched within a more conservative region, yielding a slightly higher objective.

This comparison indicates that CBDO yielded a more conservative optimum than DDO because it considered not only the constraint itself but also the confidence in satisfying that constraint under metamodel uncertainty.

TABLE II
OPTIMAL DESIGNS FROM DDO AND CBDO WITH THE 40-SAMPLE GP MODEL

Method	Optimal point	Max head X excursion $u_{hX,max}$ at optimum (mm)	NFR3+(50) at optimum
DDO	[0, 4.3]	595.3	0.008
CBDO	[56, 3.9]	602.6	0.009

Robustness assessment of the CBDO optima after additional training

Retraining the GP model with 48 samples had a negligible effect on the DDO optimum, which converged to the same design point as the initial 40-sample dataset. However, post-evaluation revealed a 2% failure probability (approximately 200 out of 10,000 Monte Carlo samples violated the constraint). Moreover, among the eight local samples used for retraining, one case exceeded the constraint (NFR3+(50) = 0.11) despite its belt limiting force differing from the DDO optimum by only 0.1 kN. Thus, while the DDO optimum remained stable in terms of design variables, it still exhibited a non-negligible risk of constraint violation under input variability.

The CBDO optimum shifted dynamically after additional training to ensure constraint satisfaction. While the optimal belt limiting force remained constant, the D-ring height shifted from approximately 56 mm to 40 mm.

When the CBDO constraints were applied to this updated 48-sample optimum, the design successfully satisfied both requirements: the median of the reliability distribution (R_m) was 0.9687, and the confidence level (CL) was 0.7864, both exceeding their prescribed target values. Fig. 6 illustrates that the updated CBDO optimum is located safely within the feasible domain. Ultimately, DDO produced a static design vulnerable to input uncertainty, while CBDO converged on a robust design satisfying confidence-based constraints. Fig. 7 details the number of iterations required to reach these respective optimal points.

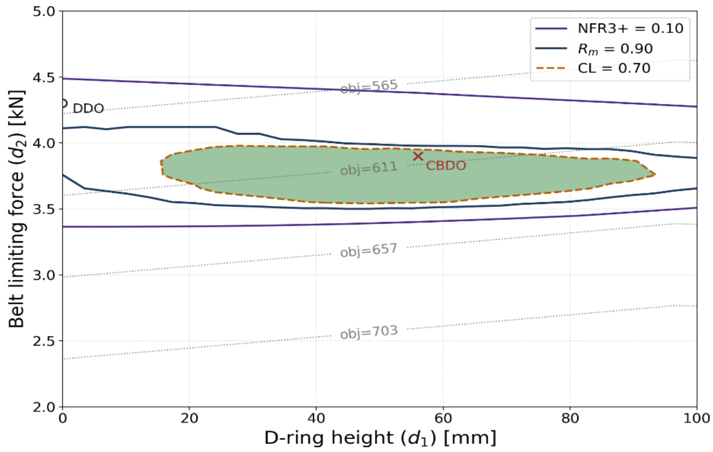

Fig. 6. Design space contours and optimal points obtained by DDO and CBDO.

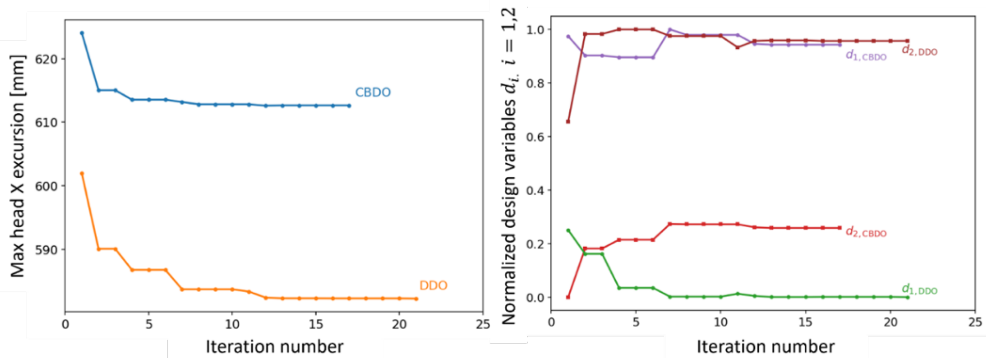

Fig. 7. Iteration histories of the objective function (*left*)and design variables for DDO and CBDO (*right*).

Table III presents the complete quantitative comparison used to verify whether the CBDO optimum accounts for metamodel uncertainty against RBDO optima across 40 and 48 samples. In the 48 samples trained model, both the RBDO and CBDO optima achieved median reliability values exceeding the target reliability of 0.90. However, the confidence level of the RBDO optimum was 0.536, which was below the prescribed target value of 0.70. This indicates that, although the RBDO optimum appeared to satisfy the reliability requirement based on the median reliability, a substantial portion of the GP posterior realisations still failed to meet the target reliability when metamodel uncertainty was explicitly propagated. In contrast, the CBDO optimum satisfied the confidence-level requirement, with $CL = 0.703$, exceeding the target value of 0.70. These results show that even after increasing the training dataset from 40 to 48 simulations, metamodel uncertainty remained non-negligible, and the CBDO framework provided a more reliable optimum by explicitly considering this uncertainty. Figs. C2 and C3 presents the visual distribution of these findings, explicitly illustrating the contrast between the 46.4% unsatisfied region left by the RBDO approach and the successful 70.3% target satisfaction achieved by the CBDO framework.

TABLE III

EVALUATION OF RELIABILITY AND CONFIDENCE LEVEL FOR RBDO AND CBDO OPTIMA

Number of Samples	Method	Reliability	Confidence Level
n = 40	RBDO	57.77%(5%tile) 82.11%(50%tile) 99.86%(95%tile)	31.38%
	CBDO	76.53%(5%tile) 95.20%(50%tile) 100.0%(95%tile)	69.99%
n = 48	RBDO	72.22%(5%tile) 90.96%(50%tile) 100.0%(95%tile)	53.64%
	CBDO	80.56%(5%tile) 93.7%(50%tile) 100.0%(95%tile)	70.32%

IV. DISCUSSION

Two GP models were trained to predict head X-excursion and NFR3+(50); their performance was assessed using leave-one-out cross-validation (LOOCV). For maximum head X excursion, the GP model yielded $R^2 = 0.75$, NRMSE = 0.006, and MAE = 20.8 mm. Most LOOCV errors were within 5%, with two outliers raising the MAE; parity plots are in Appendix C.

For NFR3+(50), the GP model yielded $R^2 = 0.81$, NRMSE = 0.50, and MAE = 0.08. The R^2value suggests that the model captures overall thoracic injury variation; the NRMSE = 0.50 reflects nonlinear, threshold-sensitive rib fracture mechanisms.

The CBDO produced a more conservative design: DDO achieved 22 mm smaller head excursion but without sufficient constraint-satisfaction margin, while CBDO satisfied the thoracic constraint, reliability, and confidence-level requirements. With the 48-sample GP model, CBDO achieved $R_m = 0.96$ and $CL = 0.78$, satisfying both target values of 0.9 and 0.7, respectively. This demonstrates that the proposed CBDO framework is both a performance optimisation method but is also an approach that ensures confidence in constraint satisfaction under uncertainty.

The DDO optimum was stable but not robust: additional simulations revealed 2% failure probability, and designs near [0, 4.4] failed under actual variability.

Post-evaluation showed that although the 48-sample RBDO optimum met median reliability, its confidence level (0.536) was below the 0.70 target, so a substantial fraction of GP posterior realisations failed. In contrast, CBDO achieved $CL = 0.703$, satisfying the confidence-level constraint. Therefore, the additional training data reduced but did not eliminate metamodel uncertainty, and the RBDO formulation remained vulnerable to an overconfident reliability assessment. These findings support the role of CBDO as a framework that explicitly accounts for metamodel uncertainty, rather than relying only on the predicted mean or median reliability. Notably, belt limiting force did not act independently but interacted with torso angle, H-point position, and D-ring height, indicating that restraint performance is governed by multivariable interactions and reinforcing the value of optimisation-based design.

In the initial 40 training simulations, several low belt-force configurations produced unexpectedly high NFR3+, driven by seat-belt spool bottoming-out. Even after correcting for bottoming-out, a clear inverse relationship between belt force and thoracic injury was not observed across all low-force cases (e.g., NFR3+ of 0.62 at 2 kN, but only 0.24 at 4.8 kN in another configuration). These non-intuitive trends confirm that thoracic injury risk is governed by coupled, non-linear multivariable interactions, underscoring the need for an optimisation-based restraint design approach.

These coupling dynamics are also illustrated by posture–restraint interaction: an initial torso angle of −7° (sternum 17°) dropped head X-excursion to 345.9 mm (CBDO) and 351.5 mm (DDO), about 42% below the mean of 602.48 mm, identifying a localized geometric configuration where posture markedly improves restraint efficiency. These findings suggest that specific combinations of restraint geometry and occupant kinematics can induce localised responses that differ from global trends. Consequently, design performance under uncertainty cannot be fully characterised by average tendencies alone, as specific realisations of uncertainty may lead to simultaneous improvements in both head excursion and thoracic injury risk.

Although overall NFR3+ prediction was satisfactory, some individual rib-strain models lacked accuracy with only 40 samples, indicating the need for adaptive sampling to improve metamodel accuracy in influential regions.

Limitations and Future Work

The simplified sled model does not fully represent a contemporary frontal impact environment, as pretensioners, airbags, and realistic seat structures are not included. The 3% standard deviations on design variables are generic assumptions, not production tolerances. Therefore, the findings should be interpreted within this selected sled condition. Extending the framework to vehicle-level simulations with broader design variables and injury metrics is necessary for practical restraint design. Future research will apply the CBDO framework to more representative environments. This includes testing front-seat configurations by incorporating specific cabin components like airbags, steering wheels, and instrument panels to derive results with greater practical design relevance. In addition, future work will examine sampling strategies that incorporate realistic, correlated occupant posture distributions.

V. CONCLUSION

In this study, we applied a confidence-based design optimisation (CBDO) framework based on GP modeling for occupant restraint design with HBMs, addressing the need for uncertainty-aware optimisation. A validated baseline model generated parametric data with torso angle, D-ring height, belt limiting force, and H-point X position as input variables, and GP metamodels were trained to predict head X excursion and NFR3+ response. Based on these metamodels, we performed CBDO to minimise head excursion while satisfying a thoracic injury constraint under uncertainty. The CBDO optimum was more conservative than the DDO optimum in objective value but satisfied the prescribed reliability and confidence-level requirements after additional data; the DDO optimum was stable in location but still allowed constraint violation under input uncertainty. These findings indicate that, under the conditions considered, GP-based CBDO is a practical approach for uncertainty-aware optimisation of occupant restraint designs.

VI. ACKNOWLEDGEMENTS

This work was partially supported by Hyundai Motor Company through the project "Development of an Injury Risk Analysis Method Considering Body-Type Uncertainty Using the GHBMC Model."

VII. REFERENCES

[1] Forman, J., Lin, H., Gepner, B., Wu, T., Panzer, M. (2018) Occupant safety in automated vehicles: Effect of seatback recline on occupant restraint – THOR & GHBMC. *Proceedings of the 2018 JSAE Annual Congress (Spring)*, 2018, Yokohama, Japan.

[2] Hu, J., Zhang, K., *et al*. (2019) Frontal crash simulations using parametric human models representing a diverse population. *Traffic Injury Prevention*, **20**(Suppl. 1): pp. S97–S105.

[3] Euro NCAP. (2022) Euro NCAP vision 2030: A safer future for mobility. Euro NCAP Publication, **1**(1): pp. 1–27.

[4] Tong, F., Wang, Y., Jian, Q., Lan, F., Chen, J. (2024) The effectiveness of swiveling seats in protecting reclined occupants in highly autonomous driving environments during frontal crashes. Applied Sciences, **14**(1): p. 349.

[5] Jo, Y., Baek, C., *et al*. (2023) Behavior and injury investigation of reclined occupants in frontal crash. Journal of Auto-vehicle Safety Association, **15**(4): pp. 95–101.

[6] Metropolis, N., Ulam, S. (1949) The Monte Carlo method. Journal of the American Statistical Association, **44**(247): pp. 335–341.

[7] Lee, D., Rahman, S. (2020) Practical uncertainty quantification analysis involving statistically dependent random variables. Applied Mathematical Modelling, **84**: pp. 324–356.

[8] Rahman, S. (2008) A polynomial dimensional decomposition for stochastic computing. International Journal for Numerical Methods in Engineering, **76**(13): pp. 2091–2116.

[9] Guo, Y., Lee, D., Kramer, B. (2025) Robust design optimization with limited data for char combustion. Struct Multidisc Optimization **68**(3): p. 59.

[10] Rasmussen, C. E., Williams, C. K. I. (2006) Gaussian Processes for Machine Learning. The MIT Press, Cambridge, MA, USA.

[11] Heinkenschloss, M., Kramer, B., Takhtaganov, T., Willcox, K. (2018) Conditional- Value-at-Risk estimation via reduced-order models. SIAM/ASA Journal on Uncertainty Quantification, **6**(4): pp. 1395–1423.

[12] Sun, W., Hu, J., *et al*. (2024) Efficient injury risk predictions for a diverse population using parametric human modeling and inducing points in gaussian processes. Traffic Injury Prevention, **25**(sup1): pp. S43–S50.

[13] Heo, J., Cho, M., Kim, T. (2024) Optimization of occupant restraint system using machine learning for THOR-M50 and Euro NCAP. Machines, **12**(1): p. 74.

[14] Lee, D., Rahman, S. (2022) Reliability-based design optimization under dependent random variables by a generalized polynomial chaos expansion. Structural and Multidisciplinary Optimization, **65**: p. 21.

[15] Jung, Y., Kang, K., Cho, H., Lee, I. (2021) Confidence-based design optimization for a more conservative optimum under surrogate model uncertainty caused by Gaussian process. Journal of Mechanical Design, **143**(9): 091701.

[16] Brumbelow, M. L., Baker, B. C., Nolan, J. M. (2007) Effects of seat belt load limiters on driver fatalities in frontal crashes of passenger cars. Paper Number 07-0067.

[17] Antona-Makoshi, J., Yamamoto, Y., *et al*. (2016) Effect of seatbelt and airbag loads on thoracic injury risk in frontal crashes considering average and small body sizes and age-dependent thoracic fragility. *Proceedings of the IRCOBI Conference,* 2016, Malaga, Spain, IRC-16-111.

[18] Meyer S.E., Nelson A.O., Hock D.A., McMillin J.T., Herbst B.R. *Assessing the Effects of Load Limiting Retractors on Occupant Motion*. *Proceedings of the IRCOBI Conference,* 2015, Paper IRC-15-21, pp. 114–125

[19] Yang, S., Zhou, Q., *et al*. (2022) A human body model based method for injury risk prediction considering occupant stature and posture. International Journal of Crashworthiness. DOI: 10.1080/13588265.2022.2109709

[20] Acosta, S. M., Ash, J. H., *et al*. (2016) Comparison of whole body response in oblique and full frontal sled tests. *Proceedings of the IRCOBI Conference*, 2016, Malaga, Spain.

[21] Crandall, J. (2015) University of Virginia Center for Applied Biomechanics. (2015) Evaluation of PMHS response in gold standard 2 frontal crash tests. Technical report, National Highway Traffic Safety Administration (NHTSA), Technical report prepared under Cooperative Agreement No. DTNH22-09-H-00247.

[22] Euro NCAP (2025) Qualification procedure for human body models crash protection. Technical Bulletin CP 550, Version 1.1, December 2025.

[23] Hartlen, D. C., Cronin, D. S. (2022) Arc-length re-parametrization and signal registration to determine a characteristic average and statistical response corridors of biomechanical data. *Frontiers in Bioengineering and Biotechnology,* **10**:843148.

[24] Parkinson, M. B., Reed, M. P. (2006) Optimizing vehicle occupant packaging. SAE Technical Paper 2006-01-0961, doi: 10.4271/2006-01-0961.

[25] Sunnevång, C., Hynd, D., Carroll, J., Dahlgren, M. (2014) Comparison of the THORAX Demonstrator and HIII sensitivity to crash severity and occupant restraint variation. Proceedings of the IRCOBI Conference, 2014, Berlin, Germany, IRC-14-42.

[26] Jakobsson, L., Bohman, K., Stockman, I., Andersson, M., Osvalder, A.-L. (2019) Rear seat safety for the growing child — A new 2-stage integrated booster cushion. Proceedings of the 26th ESV Conference, Eindhoven, Netherlands, Paper Number 19-0091.

[27] Shaw, G., Parent, D., *et al*. (2009) Impact response of restrained PMHS in frontal sled tests: Skeletal deformation patterns under seat belt loading. Stapp Car Crash Journal, **53**: pp. 1–48.

[28] Larsson, K.-J., Blennow, A., Iraeus, J., Pipkorn, B., and Lubbe, N. (2021) Rib Cortical Bone Fracture Risk as a Function of Age and Rib Strain: Updated Injury Prediction Using Finite Element Human Body Models. *Frontiers in Bioengineering and Biotechnology*, **9**:677768. doi: 10.3389/fbioe.2021.677768.

[29] Loeppky, J.L., Sacks, J., Welch, W.J. (2009) Choosing the sample size of a computer experiment: A practical guide. Technometrics, **51**(4): pp. 366–376.

[30] Helton, J. C., Davis, F. J. (2003) Latin hypercube sampling and the propagation of uncertainty in analyses of complex systems. Reliability Engineering & System Safety, **81**(1): pp. 23–69.

[31] Janssen, H. (2013) Monte-Carlo based uncertainty analysis: Sampling efficiency and sampling convergence. Reliability Engineering and System Safety, **109**: pp. 123–132.

[32] Morris, M. D., Mitchell, T. J. (1995) Exploratory designs for computational experiments. Journal of Statistical Planning and Inference **43**(3): pp. 381-402.

[33] Li, C. C., and Der Kiureghian, A. (1993) Optimal discretization of random fields. Journal of Engineering Mechanics, **119**(6): pp. 1136–1154.

VIII. APPENDIX

APPENDIX A – PARAMETRIC SIMULATION RESULTS

Baseline Model Validation Results

TABLE AI
QUANTITATIVE EVALUATION USING ARCGEN-BASED ELLIPSE & DALW SCORES

Target	Ellipse score		DALW (warpage) score	
Result [mm]	NCAP threshold	GHBM v2.3	NCAP threshold	GHBM v2.3
Head X Displacement	–	0.81	0.76	1.0
Head Y Displacement	–	1.0	0.47	1.0
Head Z Displacement	–	0.42	–	0.56
T1 X Displacement	–	0.08	0.28	0.47
T1 Y Displacement	–	0.40	0.16	0.72
T1 Z Displacement	–	0.02	–	0.03
T8 X Displacement	–	0.07	0.40	0.47
T8 Y Displacement	–	0.53	0.27	0.72
T8 Z Displacement	–	0.01	–	0.04
Pelvis X Displacement	–	0.0	0.15	0.41
Pelvis Y Displacement	–	0.55	0.39	0.87
Pelvis Z Displacement	–	0.07	–	0.16
Chest Deflection	–	0.11	0.39	0.5

TABLE AII
PARAMETRIC MODEL SIMULATION RESULTS

Case	Torso Angle (°)	D-ring *height* (mm)	Belt limiting force (kN)	H-point X position (mm)	Max head X excursion (mm)	NFR3+(50)
1	-10	72	3.3	6	652.27	0.032997
2	-10	63	2	-2	709.464	0.816513
3	-10	80	4.1	-3	568.031	0.041682
4	-10	14	3.3	7	636.564	0.137922
5	-10	52	4.7	10	510.393	0.081275
6	-10	85	2.9	-6	686.133	0.393928
7	-10	91	3	5	683.912	0.297583
8	-10	38	3.8	-10	579.938	0.095265
9	-5	27	2	-5	717.134	0.853308
10	-5	58	4.8	-2	534.452	0.05137
11	-5	64	2.4	3	719.728	0.861816
12	-5	8	2.9	2	699.789	0.571643
13	-5	17	4.5	7	544.419	0.080318
14	-5	47	3.4	-4	666.017	0.112969
15	-5	78	4.1	9	612.939	0.055779
16	5	96	3.8	-8	637.276	0.058878
17	0	59	3.2	5	726.792	0.231446
18	0	63	4.9	0	735.053	0.428365
19	0	19	3.7	-5	653.799	0.018451
20	0	8	2.5	3	740.089	0.653002
21	0	99	2.8	-1	745.265	0.755919
22	0	80	4.1	-8	636.959	0.046929
23	0	28	4.3	9	603.615	0.013546
24	0	45	2.1	-7	746.466	0.800652

25	5	84	2.4	1	720.712	0.434038
26	5	97	4.8	-2	506.892	0.306645
27	5	13	4.3	7	524.116	0.020255
28	5	13	4.2	4	532.329	0.022391
29	5	61	3.1	-7	659.42	0.00916
30	5	30	2.6	7	707.532	0.07527
31	5	11	3.1	-8	645.797	0.00208
32	5	64	3.9	9	580.101	0.015452
33	10	45	4.6	2	496	0.040661
34	10	74	2.4	7	730.269	1.79E-05
35	10	88	3.8	4	578.113	0.007503
36	10	27	3.5	-5	572.077	0.001647
37	10	34	2.4	-9	716.634	0.000821
38	10	82	4.5	5	517.371	0.0196
39	10	8	4.1	-5	522.786	0.005611
40	10	79	4.4	-5	523.862	0.046136

TABLE AIII

ADDITIONAL PARAMETRIC MODEL SIMULATION RESULTS

Method	*Case*	Torso Angle (°)	D-ring *height* (mm)	Belt limiting force (kN)	H-point X position (mm)	Max head X excursion (mm)	NFR3+(50)
DDO	1	0	0	4.3	0	580.584	0.009926
	2	1	0	4.3	-9	515.633	0.013751
	3	-3	0	4	5	535.964	0.002725
	4	3	0	4.3	-4	537.525	0.010078
	5	5	0	4.2	-8	549.83	0.017865
	6	-7	0	4.3	0	351.472	0.02671
	7	-10	0	4.4	3	508.123	0.119983
	8	-5	0	4.2	-6	550.284	0.016396
CBDO	1	10	56	3.9	-2	546.853	0.008749
	2	1	55	4	10	587.251	0.026653
	3	-7	52	4	0	345.872	0.042775
	4	10	55	4	-3	537.064	0.0103
	5	4	57	3.9	-2	605.404	0.061072
	6	-3	59	4	-10	556.778	0.003069
	7	5	55	4	6	601.438	0.089693
	8	-5	58	4	2	548.449	0.006927

APPENDIX B – SCATTER PLOTS OF INPUT VARIABLES VERSUS OUTPUT RESPONSES

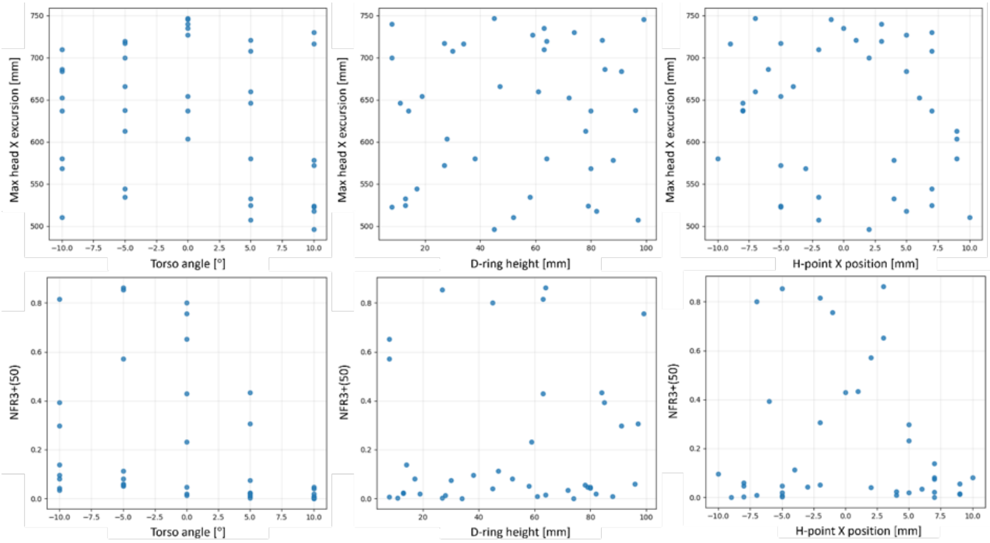

Fig. B1. Scatter plots of torso angle, D-ring height, and H-point position versus max head X excursion with bottoming out condition.

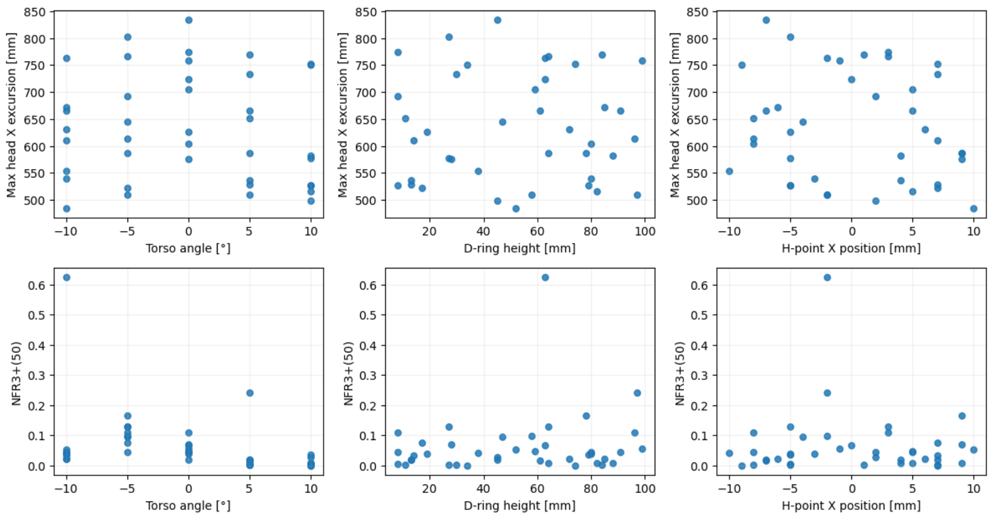

Fig. B2. Scatter plots of torso angle, D-ring height, and H-point position versus max head X excursion with non bottoming out condition.

APPENDIX C – GAUSSIAN PROCESS MODEL VALIDATION RESULTS

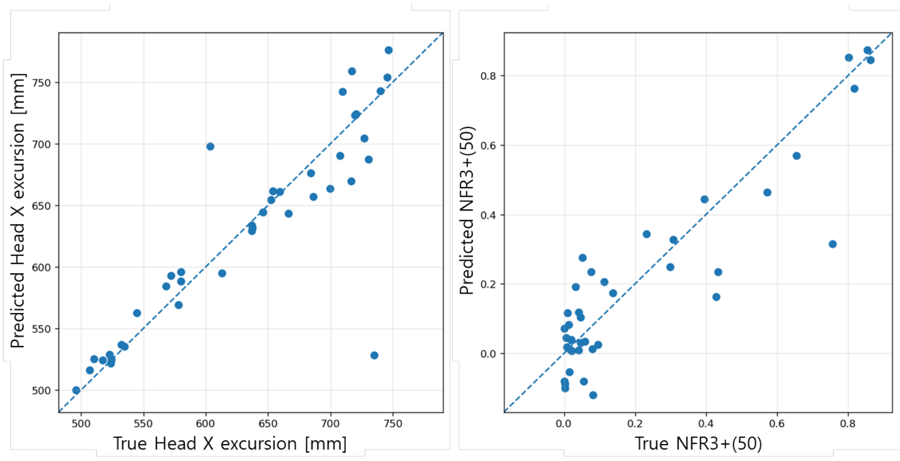

Fig. C1. LOOCV parity plots for the GP surrogate models predicting maximum head X excursion (*left*) and NFR3+(50) (*right*).

Appendix D ***Confidence-Level Comparison for RBDO and CBDO Optima***

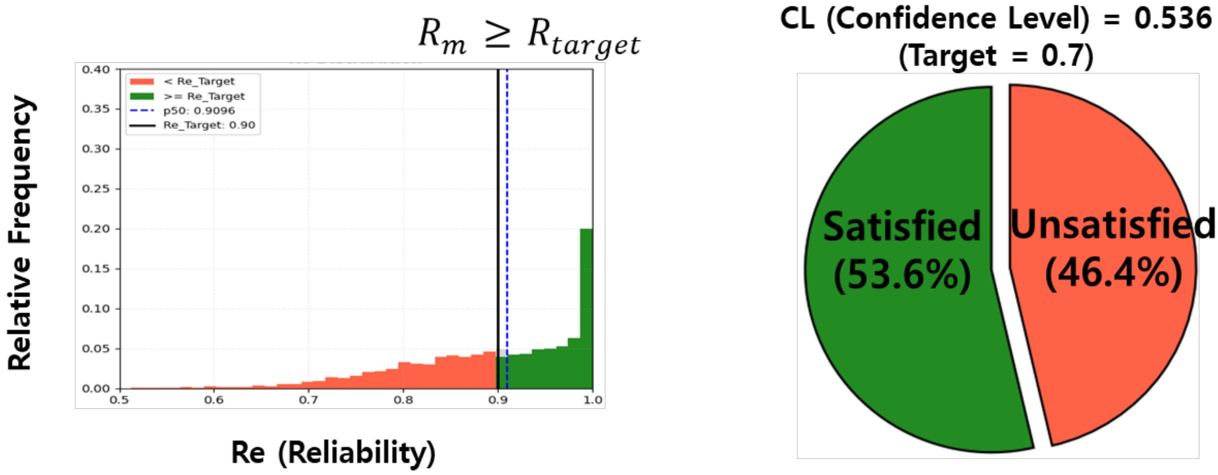

Fig. D1. Reliability distribution (*left*) and confidence level evaluation (*right*) for RBDO optimum obtained from the 48 samples trained GP model.

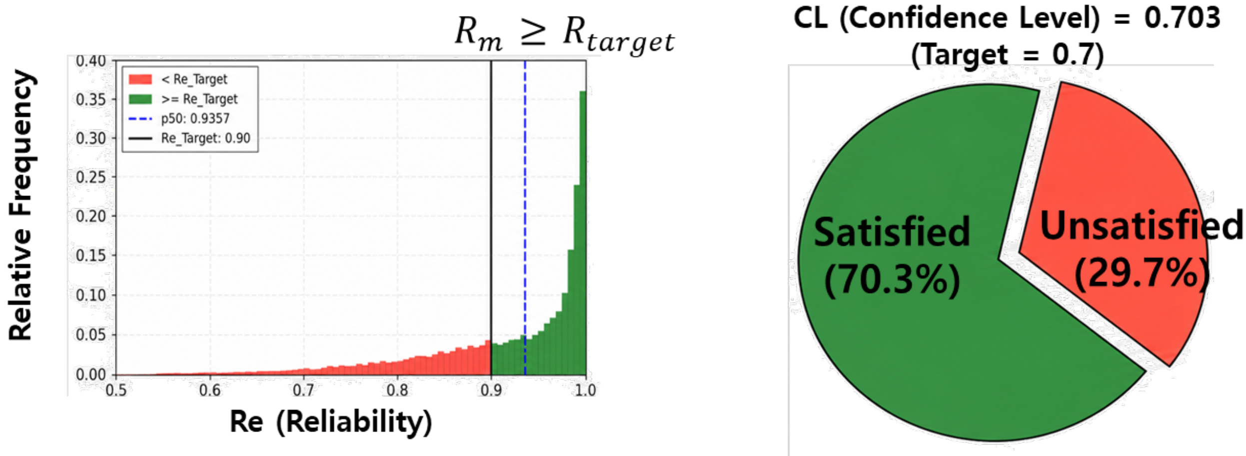

Fig. D2. Reliability distribution (*left*) and confidence level evaluation (*right*) for CBDO optimum obtained from the 48 samples trained GP model.

APPENDIX E – GAUSSIAN PROCESS MODEL

We trained the GP model to predict the injury responses or matrices, such as $u_{hX,max}$ and NFR3+(50), for uncertain input data $\boldsymbol{x} = (x_1,\, x_2, x_3, x_4)^T \in \mathbb{R}^4$, where x_1 = torso angle (°), x_2 = D-ring height (mm), x_3 = Belt limiting force (kN), and x_4 = H-point X position (mm). For given $L = 40$ input-output datasets $\{x^{(l)}, f_{hX,\max}(x^{(l)})\}_{l=1}^{L}$ and $\{x^{(l)}, f_{\mathrm{NFR3+}}(x^{(l)})\}_{l=1}^{L}$, we can assume that outputs $f_{hX,\max}(\boldsymbol{x})$ and $f_{\mathrm{NFR3+}}(\boldsymbol{x})$ follow a Gaussian Process $GP(\cdot,\cdot)$ as

$$f_{hX,max}(\boldsymbol{x}) \sim GP\left(\mu_{hX,max}(\boldsymbol{x}),\; k_{hX,max}(\boldsymbol{x},\boldsymbol{x}')\right) \qquad (E1)$$

$$f_{NFR3+}(\boldsymbol{x}) \sim GP\left(\mu_{NFR3+}(\boldsymbol{x}),\; k_{NFR3+}(\boldsymbol{x},\boldsymbol{x}')\right) \qquad (E2)$$

where, $\mu_{hX,max}(\boldsymbol{x})$ and $\mu_{NFR3+}(\boldsymbol{x})$ are the mean and $k_{hX,\max}(\boldsymbol{x},\boldsymbol{x}')$ and $k_{\mathrm{NFR3+}}(\boldsymbol{x},\boldsymbol{x}')$ are the covariance functions between two input vectors $\boldsymbol{x}$ and $\boldsymbol{x}'$ for $u_{hX,max}$ and NFR3+(50), respectively. In this study, we set the mean function to zero and adopt the Matérn kernel, i.e.:

$$k_t(\boldsymbol{x}-\boldsymbol{x}') = \sigma^2 \frac{2^{1-v}}{\Gamma(v)} \left(\frac{\sqrt{2v}\|\boldsymbol{x}-\boldsymbol{x}'\|}{l}\right)^{v} K_v\left(\frac{\sqrt{2v}\|\boldsymbol{x}-\boldsymbol{x}'\|}{l}\right),\;\; t \in \{\mathrm{u_{hX,max}}, \mathrm{NFR3{+}(50)}\}, \qquad (E3)$$

which provides flexibility in modelling complex relationships with the input data. In Eq. 4, $\|\boldsymbol{x}-\boldsymbol{x}'\|$ is a Euclidean distance between the input vector $\boldsymbol{x}$ and $\boldsymbol{x}'$, l is a length-scale parameter, v is a positive parameter, $\Gamma(\cdot)$ is a gamma function and $K_v(\cdot)$ is a modified Bessel function. The kernel parameters were optimised by minimising the LOOCV error. Since both the training outputs vector $\boldsymbol{y}$ and the output of new input vector $\boldsymbol{x}^*$ follow GP, its joint distribution is Gaussian $\mathcal{N}(\cdot,\cdot)$, i.e.:

$$\begin{bmatrix}\boldsymbol{y}\\ f(\boldsymbol{x}^*)\end{bmatrix} \sim \mathcal{N}\left(\begin{bmatrix}0\\0\end{bmatrix},\begin{bmatrix}\boldsymbol{K} & \boldsymbol{k}_*\\ \boldsymbol{k}_*^{\mathrm{T}} & k(\boldsymbol{x}^*,\boldsymbol{x}^*)\end{bmatrix}\right),\ \boldsymbol{K}=\begin{bmatrix}k(\boldsymbol{x}^{(1)},\boldsymbol{x}^{(1)}) & \cdots & k(\boldsymbol{x}^{(1)},\boldsymbol{x}^{(L)})\\ \vdots & \ddots & \vdots\\ k(\boldsymbol{x}^{(L)},\boldsymbol{x}^{(1)}) & \cdots & k(\boldsymbol{x}^{(L)},\boldsymbol{x}^{(L)})\end{bmatrix},\ \boldsymbol{k}_*=\begin{bmatrix}k(\boldsymbol{x}^{(1)},\boldsymbol{x}^*)\\ \vdots\\ k(\boldsymbol{x}^{(L)},\boldsymbol{x}^*)\end{bmatrix}. \quad (E4)$$

where, $\boldsymbol{K}\in R^{L\times L}$ is the covariance matrix computed from the training data, $\boldsymbol{k}_*\in R^{L\times 1}$ is the covariance vector between the training data and the new input vector $\boldsymbol{x}^*$, and $k(\boldsymbol{x}^*,\boldsymbol{x}^*)\in R$ is the scalar covariance at the new input vector $\boldsymbol{x}^*$. The GP model used these values to predict the injury metrics for the new input vector $\boldsymbol{x}^*$ as posterior mean and variance:

$$\tilde{\mu}(\boldsymbol{x}^*) = \boldsymbol{k}_*^{\mathrm{T}}\boldsymbol{K}^{-1}\boldsymbol{y}, \quad (E5)$$
$$\tilde{\sigma}^2(\boldsymbol{x}^*) = k(\boldsymbol{x}^*,\boldsymbol{x}^*) - \boldsymbol{k}_*^{T}\boldsymbol{K}^{-1}\boldsymbol{k}_* \quad (E6)$$

where, $\tilde{\mu}(\boldsymbol{x}^*)$ is the mean which represents the expected value, while their predictive variance, $\tilde{\sigma}^2(\boldsymbol{x}^*)$ quantifies the uncertainty in the prediction of each injury metrics of the new input vector $\boldsymbol{x}^*$such as $f_{hX,max}(\boldsymbol{x}^*)$ and $f_{\mathrm{NFR3+}}(\boldsymbol{x}^*)$. This formulation allows the GP model to provide a point prediction for the injury response and an uncertainty measure, which is particularly useful for assessing the reliability of predictions in injury risk analysis.

Appendix F – ***Parametric relationships between input variables and output responses***

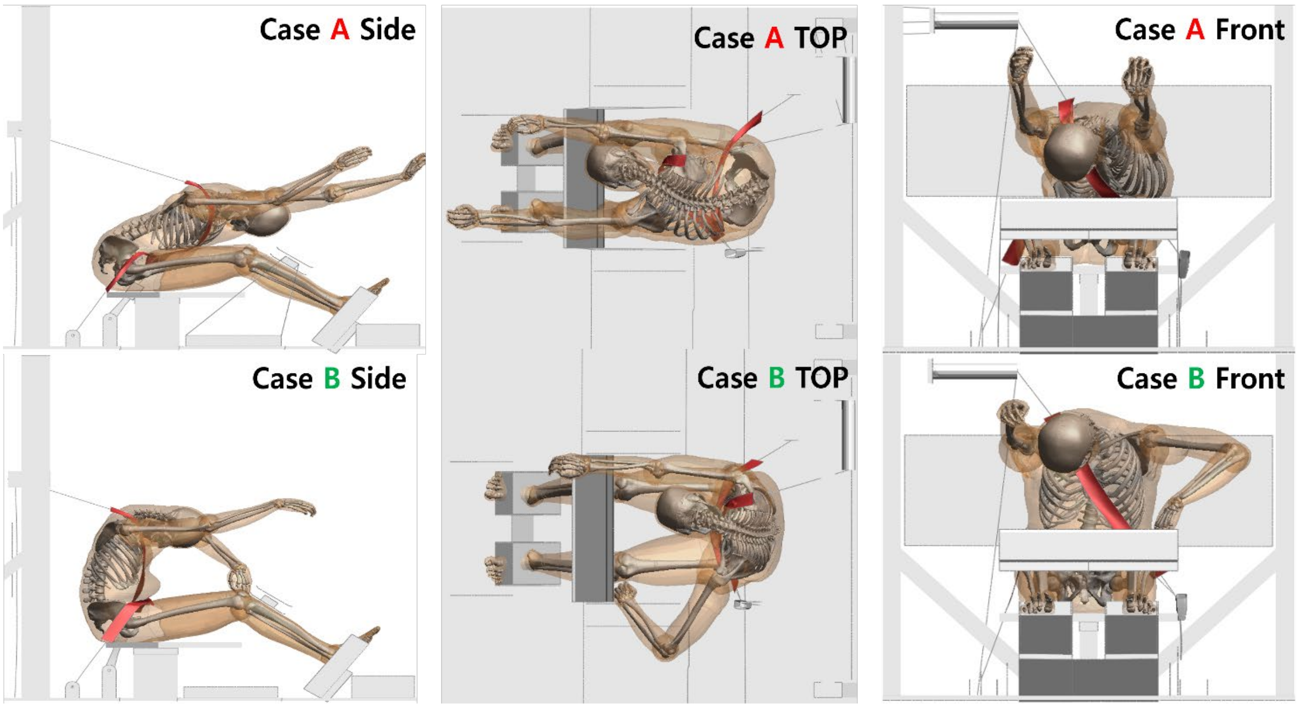

Fig. F1. Comparison of occupant kinematics between CASE A and CASE B identified in Fig. 6, shown from the side, top, and front views. In CASE A, the lower belt limiting force allowed greater belt payout and less upper-body restraint, resulting in pronounced forward flexion of the occupant. In contrast, in CASE B, the higher belt limiting force produced stronger restraint of the torso, thereby limiting forward motion while inducing a more rotational body motion about the belt.